NASA Technical Memorandum 106274

Prediction of Gas-Liquid Two-Phase Flow Regime in Microgravity

Jinho Lee and Jonathan A. Platt
Lewis Research Center
Cleveland, Ohio

July 1993

NASA

PREDICTION OF GAS-LIQUID TWO-PHASE FLOW REGIME IN MICROGRAVITY

Jinho Lee* and Jonathan Platt
National Aeronautics and Space Administration
Lewis Research Center
Cleveland, Ohio 44135

SUMMARY

An attempt is made to predict gas-liquid two-phase flow regime in a pipe in a microgravity environment through scaling analysis based on dominant physical mechanisms. Simple inlet geometry is adopted in the analysis to see the effect of inlet configuration on flow regime transitions.

Comparison of the prediction with the existing experimental data shows good agreement, though more work is required to better define some physical parameters.

The present analysis clarifies much of the physics involved in this problem and can be applied to other configurations.

1. INTRODUCTION

Currently, a single-phase fluid loop is used in the space shuttle to transport waste heat to radiators. For the much higher power levels, as high as multimegawatts, anticipated for future spacecraft, this type of system becomes prohibitively large and heavy. Due to this shortcoming, the use of two-phase fluid loops has been suggested as an alternative for the removal and transport of high waste-heat loads to space radiators (ref. 1). The design and analysis of such loops, however, requires an understanding of flow regimes, pressure drops, and heat transfer in a microgravity environment. There has been a great deal of work done on the two-phase flow problems under normal gravity during the last four decades. However, there has been little work on two-phase flow phenomena in microgravity. Reasons for the lack of studies in this area include the complex nature of multiphase flow and the great difficulty in performing experiments in a reduced gravity environment.

It can easily be seen from experiments that gravity dominantly affects the flow pattern of two-phase flow in a pipe under normal gravity (ref. 2). As the level of gravity is reduced its dominant role is diminished and, as a result, the behavior of two-phase flow in microgravity differs from that at 1-g. It is also to be noted that the entrance effect on the two-phase flow behavior is negligible under normal gravity while the entrance configuration could have pronounced effects on the flow pattern in the absence of gravity, because the presence of gravity tends to stabilize the flow and minimize the entrance effects. Since a purely analytical treatment of two-phase flow is impractical, in the present analysis, through scaling analysis based on the dominant physical mechanisms, analytical models are developed which can predict the gas-liquid two-phase flow pattern in a pipe in microgravity. Due to the importance of inlet geometry, a simple inlet configuration is adopted and the resulting flow pattern from such an inlet geometry is studied considering the evolution of the inlet region flow pattern in the downstream region.

---

*National Research Council, NASA Research Associate at Lewis Research Center.

2. BASIC EQUATIONS

For the inlet configuration considered, illustrated in figure 1, gas is introduced through a nozzle of diameter d_N located at the center of a pipe of diameter D. The gas flow emerging from the nozzle and the liquid flow in the annular space around it are essentially parallel. The volumetric flow rates of the gas and liquid are Q_g and Q_f, respectively.

Depending on the value of Q_f, the gas flow will leave the nozzle as dispersed small or large bubbles for low Q_g, and as a jet-like flow for high Q_g. The resulting flow pattern will be determined by the downstream interaction between the liquid flow and the bubble-like or jet-like gas flow. Bubble-like gas flow will be examined first; consideration will then be given to jet-like gas flow. For bubble-like flows the gas may appear as well-spaced small or large bubbles or it may appear as multiple bubbles; the size of the bubbles depends upon physical mechanisms related to the bubble formation. In normal gravity, the motion of the bubbles depends to a large extent on the orientation of the pipe with respect to gravity. In microgravity, however, not only is there no prevailing direction of gravity, but the magnitude of gravity is negligible. Thus orientation of the pipe has no meaning in microgravity.

The related forces in the formation of a bubble can be divided into two groups: the detaching forces and the attaching forces (fig. 2). Detaching forces include the buoyancy force due to density difference, F_B and the gas momentum flux (or kinetic force) coming out of the nozzle, F_K. Attaching forces include the surface tension force at the nozzle exit, F_σ and the inertial drag related to the bubble motion in the liquid, F_I. Another major force is the drag force due to the viscous liquid flow, F_D. This force can be either an attaching or detaching force depending on the relative velocity between the liquid flow and the bubble center.

In this analysis, the bubble is assumed to be spherical in shape throughout its formation and the effect of previously formed bubbles is assumed negligible. In addition, both the gas and liquid are assumed to be free of contaminants. Based on the above assumptions, each force can be written as follows:

$$\text{Buoyancy force, } F_B = \frac{\pi}{6} D_b^3 (\rho_f - \rho_g) g = (\rho_f - \rho_g) V_b g \tag{1a}$$

$$\text{Momentum flux, } F_K = \rho_g \frac{Q_g^2}{\frac{\pi}{4} d_N^2} = \rho_g \frac{Q_g^2}{A_N} \tag{1b}$$

$$\text{Surface tension force, } F_\sigma = \sigma \pi d_N f(\varphi) \tag{1c}$$

$$\text{Inertial drag, } F_I = \frac{d}{dt}\left[\left(\rho_g V_b + C_M \rho_f V_b\right) \frac{dr_b}{dt}\right] \tag{1d}$$

$$\text{Liquid viscous drag, } F_D = C_D \cdot \frac{1}{2} \rho_f U_{eff}^2 A_{eff} \tag{1e}$$

where D_b and r_b are the bubble diameter and radius, A_N is a nozzle cross section area, ρ_g and ρ_f are the densities of gas and liquid, σ is the surface tension coefficient, $f(\varphi)$ is a function of the inclined

angle of the interface at the nozzle, V_b is the bubble volume, C_M is the added mass coefficient, dr_b/dt is velocity of the fluid sphere center, and C_D is the drag coefficient given as a function of Reynolds number based on bubble diameter, $Re_B = \rho_f U_{eff} D_b/\mu_f$, where μ_f is the liquid viscosity. U_{eff} and A_{eff} are effective velocity between phases and effective projection area of the bubble, respectively.

Except when $D_b \lesssim d_N$ or when $D_b \approx D$, the bubble center motion can be described from the force balance equation by Newton's second law of motion, and the bubble size can be determined by a proper force balance at the instant of detachment. Balancing the related forces in equation (1), the force balance equation is

$$F_B + F_K + F_D = F_\sigma + F_I \tag{2a}$$

or

$$\begin{aligned} &\left(\rho_f - \rho_g\right) V_b g + \rho_g \frac{Q_g^2}{A_N} + C_D \cdot \frac{1}{2} \rho_f U_{eff}^2 A_{eff} \\ &= \sigma \pi d_N f(\varphi) + \frac{d}{dt}\left[\left(\rho_g V_b + C_M \rho_f V_b\right) \frac{dr_b}{dt}\right] \end{aligned} \tag{2b}$$

The buoyancy force is negligible in microgravity, while under normal gravity it could be either an attaching or detaching force depending on the system alignment with respect to gravity. The reason for retaining buoyancy force term in equation (2) is to properly delineate the condition under which its effect is negligible. Considering

$$V_b = Q_g t \tag{3}$$

and

$$\frac{dr_b}{dt} = U_b = \frac{Q_g}{4\pi r_b^2} \tag{4}$$

the inertial drag term of equation (2b) can be written as

$$\frac{d}{dt}\left[\left(\rho_g V_b + C_M \rho_f V_b\right) \frac{dr_b}{dt}\right] = \frac{1}{3} \rho_{eff} \frac{Q_g^2}{\pi D_b^2} \tag{5}$$

where

$$\rho_{eff} = \left(\rho_g + C_M \rho_f\right) \tag{6}$$

Bubbles during growth are connected to the nozzle by a small neck. The moving direction of the bubble center is parallel to the flow direction in the gas-liquid coflowing system and the neck of a bubble is always aligned with the flow direction. Thus the inclined angle φ is usually assumed zero at the instant of detachment and the function of inclined angle $f(\varphi)$ becomes

$$f(\varphi) = 1 \tag{7}$$

In a cross-flowing system such as gas injection into flowing liquid through holes located around the periphery of the wall, the bubble center moves during expansion normal to as well as parallel to the liquid flow direction. Considering the fact that the surface tension force always acts in the normal direction of the cutting plane, the actual contact angle has to be recalculated and thus the function of the inclined angle has components in both the parallel and normal directions. But in the case of high velocity liquid flow the parallel direction forces become dominant and the bubble size could be determined from the coflowing equation, unless the gas velocity (or gas flow rate) is very high. For details, see Kim (ref. 3).

Substituting equations (5) and (7) into equation (2b), we have

$$\begin{aligned}(\rho_f - \rho_g)V_b g + \rho_g \frac{Q_g^2}{A_N} + C_D \cdot \frac{1}{2}\rho_f U_{eff}^2 A_{eff} \\ = \sigma\pi d_N + \frac{1}{3}\rho_{eff}\frac{Q_g^2}{\pi D_b^2}\end{aligned} \tag{8}$$

2.1 Conditions Under Which Buoyancy can be Neglected

In normal gravity, the buoyancy force is the major detaching force for low liquid velocity cases. When the liquid velocity is high, the liquid drag force becomes more important and it, as well as the buoyancy force, usually control the bubble detachment. In microgravity, as the buoyancy force becomes negligible either the liquid drag force or the gas momentum flux plays a dominant role in bubble detachment. By microgravity it is thus meant herein that the following conditions, from equation (8), for liquid drag force dominant

$$\frac{(\rho_f - \rho_g)V_b g}{\frac{1}{2}C_D\rho_f U_{eff}^2 A_{eff}} \ll 1 \tag{9a}$$

and for gas kinetic force dominant

$$\frac{(\rho_f - \rho_g)V_b g}{\rho_g \frac{Q_g^2}{A_N}} \ll 1 \tag{9b}$$

are present. Whether either of these conditions applies can be made clear in the course of analysis.

Neglecting the buoyancy force term, equation (8) is written as

$$\rho_g \frac{Q_g^2}{A_N} + C_D \cdot \frac{1}{2} \rho_f U_{eff}^2 A_{eff} = \sigma \pi d_N + \frac{1}{3} \rho_{eff} \frac{Q_g^2}{\pi D_b^2} \tag{10}$$

3. APPROACH

The approach to determining the flow regime in microgravity is to ask a series of questions. The answers to these questions will determine the dominant attaching and detaching forces, the flow regime in the area of the nozzle, and what changes in flow regime will occur downstream of the nozzle.

The first question: what are the relative magnitudes of the attaching and detaching forces? The first part of the answer to this question will come in chapter 4; there three "physical conditions" (low gas flow rate, intermediate gas flow rate, and high gas flow rate) will be defined based on the ratio of momentum flux to surface tension forces. For intermediate gas flow rates, a comparison of inertial drag to viscous drag is also necessary to determine the dominant attaching and detaching forces. This comparison is made in section 7.4.

What forces are equated to determine the bubble departure size? What parameter determines the bubble departure size? These are the questions that will be tackled in section 5.1 (for low gas flow rate) and sections 6.1 and 7.1 (for intermediate gas flow rate). The bubble departure size will determine a flow regime in the vicinity of the nozzle. (For high gas flow rate a jet or jet-like flow, as opposed to discrete bubbles, will occur. Therefore a different approach, a comparison of gas and liquid velocities, will be used in section 8.1 to characterize the jet or jet-like flow.)

Do the bubbles coalesce near the nozzle? In the absence of bubble breakup, the presence of bubble coalescence is assumed to leave dispersed flow with very small bubbles unchanged, to change dispersed flow with larger bubbles to slug flow, and to change slug flow to annular flow. The prescience or absence of bubble coalescence will be addressed in sections 5.2, 6.2, and 7.2. (There is no corresponding section for high gas flow rate conditions.)

Does bubble or jet breakup occur downstream of the nozzle? The possibility of breakup due to turbulent fluctuations will be raised in sections 5.3, 6.3, 7.3, and 8.3. Turbulent fluctuations can act to place an upper limit on the bubble size.

For high gas flow rate physical condition with gas velocities much higher than liquid velocities, jet breakup due to Kelvin-Helmholtz instability can occur; this is investigated in section 8.2.

4. DETERMINATION OF PHYSICAL CONDITIONS

4.1 Low Gas Flow Rate

Kumar and Kuloor (ref. 4) studied bubble formation for a submerged nozzle in a stationary liquid column under normal gravity. They pointed out that for very small gas flow rates, surface tension is the dominant force resisting bubble detachment by buoyancy. As the gas flow rates are increased, surface tension becomes less important and the inertial drag and liquid viscous drag become the important forces resisting bubble detachment. In microgravity, when the gas flow rate is small such that its momentum flux is not enough to overcome surface tension, i.e., from equation (10) under the condition

$$\rho_g \frac{Q_g^2}{A_N} \ll \sigma \pi d_N \tag{11}$$

the only bubble detaching force is liquid drag and the resisting force against the liquid drag is the surface tension force. If the liquid drag is not strong enough to overcome surface tension, there would be no other detaching force and the bubble would grow as large as the tube diameter.

4.2 Intermediate Gas Flow Rate

When the gas volumetric flow rate increases such that the momentum flux or kinetic force of the gas leaving the nozzle is enough to overcome the surface tension force at the nozzle, but less than that resulting in a jet-like flow, either the liquid viscous drag or inertial drag against the gas momentum flux becomes important in the formation of a bubble. The physical condition for this statement can be written as

$$\rho_g \frac{Q_g^2}{A_N} \leq \sigma \pi d_N \tag{12}$$

It is assumed for the time being that the average gas velocity coming out of the nozzle is larger than the liquid superficial velocity, i.e.,

$$\frac{Q_g}{A_N} > \frac{Q_f}{A} \tag{13a}$$

or

$$\frac{Q_f}{Q_g} \frac{A_N}{A} < 1 \tag{13b}$$

The reason for this restriction, (equation (13)), is that if the liquid flow is large enough to reverse the inequality, the bubble is subject to breakup even in the formation stage due to the high liquid turbulence.

(It does not imply that the bubble velocity after detachment is larger than the liquid velocity.) The necessity of this assumption will be addressed later, in Section 7.4.

4.3 High Gas Flow Rate

When the gas flow rate is very high, the gas inertia is greater than surface tension. This is represented as

$$\rho_g \frac{Q_g^2}{A_N} > \sigma \pi d_N \tag{14}$$

5.0. LOW GAS FLOW RATE $\left(\text{FIRST PHYSICAL CONDITION, } \rho_g \left(Q_g^2/A_N\right) \ll \sigma \pi d_N\right)$

5.1 Force Balance and Departure Size

Under the applicable condition (eq. (11)), we may balance the liquid drag with the surface tension force term in equation (10) as

$$C_D \frac{1}{2} \rho_f U_{eff}^2 A_{eff} = \sigma \pi d_N \tag{15}$$

For low gas flow rate and $A_N/A \ll 1$, we may put

$$U_{eff} = U_f = \frac{Q_f}{A\left(1 - \frac{A_N}{A}\right)} \approx \frac{Q_f}{A} \tag{16}$$

Expressing the effective area of bubble, A_{eff}, as

$$A_{eff} = \frac{\pi}{4}\left(D_b^2 - d_N^2\right) \tag{17}$$

the force balance in equation (15) gives

$$D_b = \left[d_N^2 + \frac{8}{C_D} \frac{\sigma d_N}{\rho_f \left(\frac{Q_f}{A}\right)^2}\right]^{1/2} \tag{18}$$

It can be seen from equation (18) that for very small gas flow rate the bubble size increases with increasing interfacial tension, but is more influenced by the liquid flow rate. The higher the superficial liquid velocity, the smaller the bubble size, as is expected. Also note that the bubble size depends on the nozzle diameter.

Dividing equation (18) by pipe diameter, D

$$\frac{D_b}{D} = \left[\left(\frac{d_N}{D}\right)^2 + \left(\frac{8}{C_D}\right)\left[\frac{\sigma}{\rho_f\left(\frac{Q_f}{A}\right)^2 D}\right]\left(\frac{d_N}{D}\right)\right]^{1/2} \tag{19}$$

Since $(d_N/D)^2 \ll 1$, $D_b/D < 1$ when

$$\left(\frac{8}{C_D}\right)^{1/2}\left[\frac{\sigma}{\rho_f\left(\frac{Q_f}{A}\right)^2 D}\right]^{1/2}\left(\frac{d_N}{D}\right)^{1/2} < 1 \tag{20}$$

and $D_b/D \geq 1$ when

$$\left(\frac{8}{C_D}\right)^{1/2}\left[\frac{\sigma}{\rho_f\left(\frac{Q_f}{A}\right)^2 D}\right]^{1/2}\left(\frac{d_N}{D}\right)^{1/2} \geq 1 \tag{21}$$

Under the condition from equation (21), the gas leaves the nozzle as a big bubble, its diameter comparable to the pipe diameter. Physically it is not possible for the bubble diameter to be larger than the pipe diameter as is implied by $D_b/D \geq 1$, but for sufficiently low liquid flow rate the bubble may elongate in the direction of flow with its length larger than the pipe diameter. As the big bubbles that can occur at low liquid flow rate are not subject to breakup into smaller ones by high liquid turbulent fluctuations, slug flow would result. The length of bubbles in this case may be the tube diameter or many times larger than that depending on the liquid flow rate. Based on this argument the criterion for bubble-slug flow transition is set as

$$\left(\frac{8}{C_D}\right)^{1/2}\left[\frac{\sigma}{\rho_f\left(\frac{Q_f}{A}\right)^2 D}\right]^{1/2}\left(\frac{d_N}{D}\right)^{1/2} = 1 \tag{22a}$$

or in terms of Weber number based on liquid superficial velocity and pipe diameter

$$\left(\frac{8}{C_D}\right)^{1/2} We^{-1/2} \left(\frac{d_N}{D}\right)^{1/2} = 1 \tag{22b}$$

It is seen from the above relation how the nozzle diameter affects the transition criterion. It is expected that at the value of liquid volumetric rate Q_f which is slightly larger than the value given by the criterion from equation (22), the flow regime may not be a dispersed flow regime characterized by small, discrete bubbles but instead may be a simple bubble flow characterized by the presence of both small and large bubbles. The demarcation between the two is not clear. It is thus preferred to designate a dispersed flow regime for the situation of $D_b/D < 1$.

5.1a An Alternative Formulation for Departure Size

As is indicated by equation (19), for low liquid flow rate the bubble may grow much larger than the nozzle diameter. Depending on the growing bubble size, the effective velocity U_{eff} over the bubble may increase and differ appreciably from the simple liquid superficial velocity given in equation (16), which in turn may prompt the earlier detachment of bubble with a reduced size, especially in a small diameter pipe. To consider this, instead of the liquid superficial velocity used in equation (16), the effective velocity could be taken to be

$$U_{eff} = \frac{Q_f}{A\left[1 - \left(\frac{D_b}{D}\right)^2\right]} \tag{23}$$

With the above effective velocity, from the force balance in equation (15) for $(d_N/D)^2 \ll 1$, the relative bubble size is given as

$$\frac{D_b}{D} = \left[1 + \frac{1 - \sqrt{4 \cdot \frac{8}{C_D} \frac{\sigma}{\rho_f \left(\frac{Q_f}{A}\right)^2 D} \frac{d_N}{D}}}{2 \cdot \frac{8}{C_D} \cdot \frac{\sigma}{\rho_f \left(\frac{Q_f}{A}\right)^2 D} \cdot \frac{d_N}{D}}\right]^{1/2} \tag{24}$$

From the above relation, it can be shown that

$$\frac{D_b}{D} < 1 \qquad \text{for} \qquad \frac{8}{C_D} \frac{\sigma}{\rho_f \left(\frac{Q_f}{A}\right)^2 D} \frac{d_N}{D} \ll 1 \tag{25}$$

and

$$\frac{D_b}{D} \to 1 \qquad \text{for} \qquad \frac{8}{C_D} \frac{\sigma}{\rho_f \left(\frac{Q_f}{A}\right)^2 D} \frac{d_N}{D} \gg 1 \tag{26}$$

Comparison shows that the condition from equation (25) for the presence of dispersed flow is almost the same as the condition from equation (20), but the condition from equation (26) is rather different from the condition from equation (21) for the presence of slug flow. According to the condition set forth in equation (21), the bubble can grow as large as pipe diameter at some low value of liquid volumetric flow rate while this is not possible under the condition set forth in equation (26), unless the liquid volumetric flow rate is vanishingly small. The condition from equation (26), in addition, cannot predict explicitly the dispersed-slug flow transition criterion. Until an experiment makes it clear which of the two is better, the transition criterion from equation (22) will be used.

5.2 Bubble Coalescence in the Nozzle Region

Some criteria for the bubble coalescence were given for stationary bubble formation system (refs. 5 to 7). In the present situation, the bubble formed at the nozzle exit is carried downstream by the liquid flow. Thus if we neglect the slip between the liquid and bubble, the gas bubble would have the same velocity as the local liquid velocity. By comparing the time for the first bubble to move one bubble diameter, D_b/U_b, with the next bubble formation time, V_b/Q_g, the condition for which bubbles will merge is

$$\frac{D_b}{U_b'} > \frac{V_b}{Q_g} \tag{27}$$

If

$$U_b' = U_f = \frac{Q_f}{A} \tag{28}$$

which means that the bubble moves with the average, or superficial, liquid velocity, equation (27) becomes

$$\frac{Q_g}{Q_f} > \frac{2}{3}\left(\frac{D_b}{D}\right)^2 \tag{29}$$

If $Q_g/Q_f < 2/3$ (consistent with low gas flow rate), since $D_b/D \leq 1$, equation (29) is never satisfied and no bubble coalescence occurs.

5.3 Breakup Due to Liquid Turbulence

The splitting of bubbles or drops in turbulent flow occurs due to the interaction of surface tension, viscous, and inertia forces. When the bubble or drop size is much smaller than the Kolmogorov microscale, defined as the length scale of the flow where viscous forces become influential, the viscous force plays a dominant role in breakup of bubbles and drops. But when the Reynolds number of the external flow field is large, as is the case in most practical applications, the spatial dimensions of such local regions are very small compared with the bubble or drop size. The determining factor for bubble or drop breakup becomes the dynamic pressure caused by velocity changes over distances on the order of the bubble or drop diameter. When the viscosity of the dispersed phase is much larger than that of the continuous phase, the effect of flows inside the drop or bubble becomes important.

The dynamic pressure due to turbulent fluctuation is

$$F_t = \frac{1}{2}\rho_f U'^2 \tag{30}$$

where U' is the velocity of most rapid eddy which can be, according to Levich (ref. 8), approximated as a frictional velocity,

$$U' = \sqrt{\frac{f}{2}}\, U_f \tag{31}$$

where f in this equation is the friction coefficient predicted by the Blasius equation

$$f = 0.046\left(\frac{\rho_f U_f D}{\mu_f}\right)^{-0.2} \tag{32}$$

The capillary pressure due to interfacial tension for a bubble of diameter D_b is

$$F_\sigma = \frac{2\sigma}{r_b} = \frac{4\sigma}{D_b} \tag{33}$$

The breakup of the bubble is expected to occur when the dynamic pressure due to turbulent fluctuations exceeds the capillary pressure. Thus from equations (30) to (33), this condition is given as

$$\frac{f}{16}\,\frac{\rho_f U_f^2 D}{\sigma}\,\frac{D_b}{D} > 1 \tag{34}$$

Substituting equation (19) into equation (34), keeping in mind that $\left(d_N/D\right)^2 \ll 1$, the condition for turbulent breakup becomes:

$$\left(\frac{C_D}{15{,}100}\right) We \left(\frac{d_N}{D}\right) Re^{-2/5} > 1 \tag{35}$$

where Re is the Reynolds number based on average liquid velocity and tube diameter, $Re = \rho_f U_f D/\mu_f$. Since $Re > 1$ and $d_N/D < 1$, this condition will not be met for any reasonable values of Weber number. The possibility, for this physical condition, of breakup of bubbles due to turbulent fluctuations is thus dismissed.

6. INTERMEDIATE GAS FLOW RATE $\left(\text{SECOND PHYSICAL CONDITION, } \rho_g\left(Q_g^2/A_N\right) \le \sigma\pi d_N\right)$,

VISCOUS DRAG CASE

Under the condition of equation (12), the liquid viscous drag opposes gas bubble detachment and is thus negative. Equation (10) then becomes

$$\rho_g \frac{Q_g^2}{A_N} = \sigma\pi d_N + C_D \cdot \frac{1}{2}\,\rho_f\, U_{eff}^2\, A_{eff} + \frac{1}{3}\,\rho_{eff}\,\frac{Q_g^2}{\pi D_b^2} \tag{36}$$

Since the inertial drag becomes more important for higher gas flow rate, the balance of gas momentum flux with liquid viscous drag is considered first. (The limits for this case are considered in section 7.4.)

6.1 Force Balance and Departure Size

Under the condition that the gas momentum flux balances liquid viscous drag, from equation (36)

$$\rho_g \frac{Q_g^2}{A_N} = \frac{C_D}{2}\,\rho_f\, U_{eff}^2\, A_{eff} \tag{37}$$

Since

$$U_{eff} = U_b - U_f$$
$$= \frac{Q_g}{\pi D_b^2}\left[1 - 4\,\frac{Q_f}{Q_g}\left(\frac{D_b}{D}\right)^2\right] \tag{38}$$

and $A_{eff} = (\pi/4)D_b^2$, from equations (37) and (38),

$$D_b = \left(\frac{C_D}{32}\,\frac{\rho_f}{\rho_g}\right)^{1/2} d_N\left[1 - 4\,\frac{Q_f}{Q_g}\left(\frac{D_b}{D}\right)^2\right] \tag{39}$$

or

$$\frac{D_b}{D} = \left(\frac{C_D}{32}\,\frac{\rho_f}{\rho_g}\right)^{1/2} \frac{d_N}{D}\left[1 - 4\,\frac{Q_f}{Q_g}\left(\frac{D_b}{D}\right)^2\right] \tag{40}$$

This is a quadratic equation for the relative bubble size, D_b/D. The solution is expressed as

$$\frac{D_b}{D} = \frac{1}{2A_qB_q}\left(\sqrt{1 + 4A_q^2 B_q} - 1\right) \tag{41}$$

where

$$A_q = \left(\frac{C_D}{32}\,\frac{\rho_f}{\rho_g}\right)^{1/2} \frac{d_N}{D} \tag{42}$$

$$B_q = 4\,\frac{Q_f}{Q_g} \tag{43}$$

From equation (41), according to the parametric value of $4A_q^2 B_q$, the relative bubble size can be given as follows:

$$\text{(i)} \qquad 4A_q^2 B_q \gg 1 \qquad \text{or} \qquad \frac{C_D}{2}\,\frac{\rho_f}{\rho_g}\,\frac{Q_f}{Q_g}\,\frac{A_N}{A} \gg 1 \tag{44}$$

$$\frac{D_b}{D} = \frac{1}{\sqrt{B_q}} = \frac{1}{2}\sqrt{\frac{Q_g}{Q_f}} \tag{45}$$

(ii) $$4A_q^2 B_q = 1 \quad \text{or} \quad \frac{C_D}{2}\frac{\rho_f}{\rho_g}\frac{Q_f}{Q_g}\frac{A_N}{A} = 1 \tag{46}$$

$$\frac{D_b}{D} = \frac{\sqrt{2}-1}{2}\sqrt{\frac{Q_g}{Q_f}} \tag{47}$$

(iii) $$4A_q^2 B_q \ll 1 \quad \text{or} \quad \frac{C_D}{2}\frac{\rho_f}{\rho_g}\frac{Q_f}{Q_g}\frac{A_N}{A} \ll 1 \tag{48}$$

$$\frac{D_b}{D} = \left(\frac{C_D}{32}\frac{\rho_f}{\rho_g}\right)^{1/2}\frac{d_N}{D} \tag{49}$$

Consider different values for $4A_q^2 B_q$. From equation (13), $(Q_f/Q_g)(A_N/A) < 1$; considering slow bubble formation, for $1 \leq Re_B \leq 10$, C_D ranges between $2.64 \leq C_D \leq 18.3$ (ref. 9); and for gas-liquid two-phase flow $\rho_f/\rho_g \gg 1$. Thus $4A_q^2 B_q = (C_D/2)(\rho_f/\rho_g)(Q_f/Q_g)(A_N/A) > 1$ (or $\gg 1$).

The bubble size therefore can be represented as

$$\frac{D_b}{D} = K_a\sqrt{\frac{Q_g}{Q_f}} \tag{50}$$

where K_a is a constant. From equations (45) and (47), $0.2 < K_a \leq 0.5$, depending on the value of $4A_q^2 B_q$. For $4A_q^2 B_q > 1$, K_a may be approximated at 0.4 without appreciable error for gas-liquid systems, which are of concern here. Equation (50) thus becomes

$$\frac{D_b}{D} = 0.4\sqrt{\frac{Q_g}{Q_f}} \tag{51}$$

Note that in the present case the nozzle diameter has no relevance in determining bubble size. For

$$\sqrt{\frac{Q_f}{Q_g}} > 0.4 \tag{52}$$

$D_b/D < 1$ and the flow is expected to be a dispersed flow unless bubble coalescence occurs. For

$$\sqrt{\frac{Q_f}{Q_g}} \leq 0.4 \tag{53}$$

$D_b/D \geq 1$ and slug flow is expected unless bubble coalescence occurs.

6.2 Bubble Coalescence in the Nozzle Region

Substituting the expression for D_b/D from equation (51) into equation (29), it is found that equation (29) is identically satisfied. This indicates that bubble coalescence always occurs in both dispersed and slug flow regimes in this situation. As a result of bubble coalescence, dispersed flow with moderately larger bubbles may change into slug flow and slug flow with long bubbles may change into annular flow, if there is no breakup due to high liquid turbulence.

6.3 Breakup Due to Liquid Turbulence

Substituting equations (32) and (51) into equation (34) gives the bubble breakup condition

$$We > 870 \sqrt{\frac{Q_f}{Q_g}}\, Re^{1/5} \tag{54}$$

Under the condition of equation (54), the bubble is expected to break up into smaller ones until it reaches its critical diameter proposed by Hinze (ref. 10) and Sevik and Park (ref. 11) (see the appendix), and the flow would be a dispersed flow unless the void fraction exceeds its critical value for dispersed to slug flow transition. Normally the criterion for bubbly to slug flow transition is given by the average critical void fraction at a cross section. For the present inlet geometry where the nozzle is located at the center of geometry, the bubbles are concentrated in the central region of the tube. For this case the transitional void fraction may become less than the void fraction averaged over the cross section. With bubble coalescence and breakup processes included, it is thus not possible to obtain a proper critical void fraction from the scaling analysis. What is anticipated is that with bubble breakup, bubbles would evenly be redistributed throughout the cross section and that the critical value of the void fraction would be close to the cross section average value. Based on the measurements of bubble size distributions at the inlet and outlet locations of the tube, Colin et al. (ref. 12) reported that the higher liquid turbulence levels in a large tube may enhance bubble coalescence more than they cause bubble breakup. It was also suggested that the absence of eddy shedding from the back of bubble could enhance coalescence and suppress the breakup. This phenomenon, however, needs more detailed study.

For current gas flow rates, bubble coalescence always occurs irrespective of the value of void fraction. When bubble breakup occurs due to strong liquid turbulence (under the condition from eq. (54)), dispersed flow would remain dispersed, but with finer bubbles, while slug flow would either remain as a slug flow, with distorted large bubbles, or would transform into churn flow with the breakdown of large bubbles.

When the bubble breakup process does not occur, we have the condition

$$We \leq 870 \sqrt{\frac{Q_f}{Q_g}}\, Re^{1/5} \tag{55}$$

Under this condition, unless $D_b/D \ll 1$, that is, unless

$$\sqrt{\frac{Q_f}{Q_g}} \gg 0.4\ , \tag{56}$$

dispersed flow would become slug flow under the condition of equation (52) and slug flow would become annular flow under the condition of equation (53).

7. INTERMEDIATE GAS FLOW RATE $\left(\text{SECOND PHYSICAL CONDITION, } \rho_g\left(Q_g/A_N\right) \leq \sigma\pi d_N\right)$, INERTIAL DRAG CASE

7.1 Force Balance and Departure Size

Consider the balance between the gas momentum flux and the inertial drag during bubble formation. Equating these two forces from equation (36), we have

$$\rho_g \frac{Q_g^2}{A_N} = \frac{1}{3}\, \rho_{eff} \frac{Q_g^2}{\pi D_b^2} \tag{57}$$

From the above relation, the bubble diameter is

$$D_b = \frac{1}{2\sqrt{3}} \left(\frac{\rho_{eff}}{\rho_g}\right)^{1/2} d_N \tag{58}$$

As $\rho_{eff}/\rho_g = 1 + C_M\,(\rho_f/\rho_g)$ from equation (6),

$$\frac{D_b}{D} = \frac{1}{2\sqrt{3}} \left(1 + C_M \frac{\rho_f}{\rho_g}\right)^{1/2} \frac{d_N}{D} \tag{59}$$

It is seen from equation (59) that the nozzle diameter is important in determining the bubble size. If

$$\left(1 + C_M \frac{\rho_f}{\rho_g}\right)^{1/2} \frac{d_N}{D} < 2\sqrt{3} \tag{60}$$

then $D_b/D < 1$ and the flow would be dispersed flow unless coalescence occurs. Or, if

$$\left(1 + C_M \frac{\rho_f}{\rho_g}\right)^{1/2} \frac{d_N}{D} \geq 2\sqrt{3} \tag{61}$$

so that $D_b/D \geq 1$, then slug flow is expected, again unless coalescence occurs.

7.2 Bubble Coalescence in the Nozzle Region

Applying equations (29) and (59), the condition of bubble coalescence is

$$\frac{Q_g}{Q_f} \frac{A}{A_N} > \frac{1}{18} \left(1 + C_M \frac{\rho_f}{\rho_g}\right) \tag{62}$$

The inertial drag becomes important over liquid viscous drag under the condition

$$\frac{Q_g}{Q_f} \frac{A}{A_N} > 0.025\ C_D \frac{\rho_f}{\rho_g} \tag{63}$$

(This will be shown in section 7.4.) For $C_M = 11/16$ and $C_D \geq 1.5$ (see "Comparisons and Discussions" section), meeting this condition implies that equation (62) is satisfied and therefore that bubble coalescence always occurs.

7.3 Breakup Due to Liquid Turbulence

From equations (34) and (59), the condition for bubble breakup is given as

$$We > \frac{1205}{\left(1 + C_M \frac{\rho_f}{\rho_g}\right)^{1/2}} \left(\frac{d_N}{D}\right)^{-1} Re^{1/5} \tag{64}$$

When bubble breakup does not occur, the condition

$$We \leq \frac{1205}{\left(1 + C_M \frac{\rho_f}{\rho_g}\right)^{1/2}} \left(\frac{d_N}{D}\right)^{-1} Re^{1/5} \tag{65}$$

must be satisfied. For the above condition, a slug flow is expected under the condition of equation (60) and an annular flow under the condition of equation (61). From equation (59), $D_b/D \ll 1$ for

$$\left(1 + C_M \frac{\rho_f}{\rho_g}\right)^{1/2} \frac{d_N}{D} \ll 2\sqrt{3} \tag{66}$$

and a dispersed flow is expected under this condition even though bubble coalescence occurs.

When both bubble coalescence and bubble breakup occur, we expect a dispersed flow with finer bubbles under the condition of equation (60); a slug flow with distorted large bubbles or a churn flow with disrupted large bubbles is expected under the condition of equation (61).

7.4 Comparison of Liquid Viscous Drag to Inertial Drag

Now consider the criterion under which the inertial drag becomes more important than the liquid viscous drag. From equation (36), by comparing the magnitude of each term, the inertial drag becomes important when

$$\frac{C_D}{2} \rho_f U_{eff}^2 A_{eff} < \frac{1}{3} \rho_{eff} \frac{Q_g^2}{\pi D_b^2} \tag{67}$$

Substituting U_{eff} from equation (38) and $A_{eff} = (\pi/4)D_b^2$ into equation (67) and rearranging terms gives

$$\frac{C_D}{8}\,\rho_f\left(\frac{D}{D_b}\right)^2\left[1-4\,\frac{Q_f}{Q_g}\left(\frac{D_b}{D}\right)^2\right]^2 < \frac{1}{3}\,\rho_{eff}\left(\frac{D}{D_b}\right)^2 \tag{68}$$

Substituting the proper expression for D_b/D in each side of equation (68), that is, D_b/D from equation (51) to the left-hand side and D_b/D from equation (61) to the right-hand side of the above inequality and with $\rho_{eff} = (\rho_g + C_M\rho_f)$, we have the following condition for the importance of the inertial drag over the liquid drag

$$\frac{Q_g}{Q_f}\,\frac{A}{A_N} > 0.025\;C_D\,\frac{\rho_f}{\rho_g} \tag{63}$$

The liquid viscous drag becomes important when

$$\frac{Q_g}{Q_f}\,\frac{A}{A_N} \leq 0.025\;C_D\,\frac{\rho_f}{\rho_g} \tag{69}$$

Prior to this analysis, it was assumed that $(Q_f/Q_g)\,(A_N/A) < 1$ (eq. (13)). This condition restricts the liquid flow rate in order to analyze the problem without bubble breakup. When the liquid flow rate is high enough to satisfy the bubble breakup condition (eq. (54)), equation (13) may not be satisfied. Since the explicit condition is given above for the importance of liquid viscous drag (eq. (69)) and since equation (54) supersedes equation (13), equation (13) is no longer a necessary condition.

8. HIGH GAS FLOW RATE $\left(\text{THIRD PHYSICAL CONDITION, } \rho_g\left(Q_g^2/A_N\right) > \sigma\pi d_N\right)$

8.1 Determination of Jet Velocity

In this case the net forward kinetic force of the gas is large enough to overcome the interfacial tension force and to by itself cause detachment. To be more precise, the kinetic force is sufficient to push the gas bubble forward before the bubble becomes large. As a result, the gas flow is no longer a stream of bubbles. It is instead either a jet-like flow due to strong bubble coalescence or a jet flow. The occurrence of bubble coalescence can be seen easily from equation (27), where the bubble coalescence condition is identically satisfied when the bubble velocity for this case, $U_b = Q_g/\pi D_b^2$, is substituted.

In jet flow the interfacial friction between the gas and liquid becomes important, while in jet-like flow the resisting force against the gas flow would be the total drag for the bubble motion through the liquid neglecting bubble coalescence. The second case will be addressed first.

For high gas flow rates, the bubble shape would be deformed into a nonspherical shape. But for simplicity, assuming a spherical bubble shape, from equation (36), we may balance the gas kinetic force with the liquid viscous drag as

$$\rho_g \frac{Q_g^2}{A_N} = C_D \cdot \frac{1}{2} \rho_f U_{eff}^2 A_{eff}$$

$$= \frac{C_D}{8} \rho_f \frac{Q_g^2}{\pi D_b^2} \left[1 - 4 \frac{Q_f}{Q_g} \left(\frac{D_b}{D}\right)^2\right]^2 \tag{70}$$

Since bubble diameter is expected to be comparable with nozzle diameter for high gas flow rates,

$$4 \frac{Q_f}{Q_g} \left(\frac{D_b}{D}\right)^2 \ll 1 \tag{71}$$

With this condition, equation (70) reduces to

$$\frac{D_b}{D} = \left(\frac{C_D}{32} \frac{\rho_f}{\rho_g}\right)^{1/2} \frac{d_N}{D} \tag{72}$$

For high velocity bubble motion and if the bubbles are free of surface-active contaminants, $C_D \lesssim 1.0$ for $Re_B \geq 30$. Thus even though $\rho_f/\rho_g \gg 1$ for gas-liquid two-phase flow, $D_b/D < 1$ is expected. Since the gas flow appears as a jet-like flow due to strong bubble coalescence, the bubble diameter should be indicative of the jet diameter, and the flow regime would very much depend on the jet flow characteristics. For normal gravity there exist a few correlations for the velocity below which the jet would not form. Smith and Moss (ref. 13) found that for liquids injected into gases, the jetting velocity, U_J, could be given by

$$U_J = K_J \left(\frac{\sigma}{\rho_d d_N}\right)^{1/2} \tag{73}$$

where K_J was determined experimentally to be between 2.0 and 3.0, and ρ_d is the density of the dispersed phase. Scheele and Meister (ref. 14) have shown that for a flat (or average) velocity profile for the dispersed phase, the jetting velocity is given by the equation

$$U_J = 2.0 \left[\frac{\sigma}{\rho_d d_N}\left(1 - \frac{d_N}{d_F}\right)\right]^{1/2} \tag{74}$$

where d_F is the diameter of the drop which would form at the nozzle velocity U_J if a jet did not form. No explicit relation is available for the gas-liquid system which may render a more quantitative criterion than the condition of equation (73).

8.2 Breakup Due to Kelvin-Helmholtz Instability

In a jet flow, disturbances appear on the jet surface and move at the velocity of interface. When the most unstable disturbance grows, it leads to the disruption of the jet, breaking it up into very fine bubbles in the case of gas jet flow or fine drops in the liquid jet flow case. It is noted by Ostrach and Koestel (ref. 15) that from the Kelvin-Helmholtz stability criterion, annular two-phase flow in a zero-gravity environment is unstable to disturbances of all wavelengths if the effect of surface tension is neglected, no matter how small the velocity difference or shear of the two fluids. In an internal flow, one part of the fluid layer can produce disturbances to another part and these disturbances may accumulate in varied nonlinear ways. Thus the question is raised as to whether conventional linear stability analyses such as the Kelvin-Helmholtz stability criterion have any meaning for this type of internal flow.

Usually linear stability theory is used to predict jet length from jet inception to disruption. Meister and Scheele (ref. 16) showed that the jet length, L_J, can be expressed as

$$L_J = K_J \frac{U_I}{\alpha} \ln\left(\frac{a_N}{\xi_O}\right) \tag{75}$$

where K_J is a constant, α is the disturbance growth rate, U_I is the interfacial velocity, a_N is the jet radius at the nozzle exit, and ξ_o is the initial amplitude of the most unstable disturbances. In the case of liquid jets in gas, the gas phase exerts negligible friction on the liquid jet and disturbances at the interface move at the same speed as the liquid, and the jet forms easily. However, in the liquid-liquid and gas-liquid systems, the interfacial friction is significant and the interfacial velocity is low enough that the most unstable disturbance amplifies to the nozzle radius within a short distance from the nozzle exit. When the nozzle diameter is very small, the jet radius, a_N, is also very small. From equation (75), as $\ln(a_N/\xi_O) \ll 1$, either the jet length would be very small or else there would be no jet formation at nozzle exit. If no jet forms there would be a mist flow of very fine bubbles and drops due to the disruption and atomization of the jet; this was observed by Leibson et al. (ref. 17) and Hayworth and Treybal (ref. 18).

In the present analysis, it is speculated that the length over which the jet persists can be estimated by balancing the interfacial friction between gas jet and liquid flow with the gas kinetic force. Using equation (36), with the liquid viscous drag regarded as the interfacial drag, the balance of interfacial drag and gas kinetic force is expressed as

$$\rho_g \frac{Q_g^2}{A_N} = C_{fi} \cdot \frac{1}{2} \rho_g \left(U_g - U_f\right)^2 A_i \tag{76}$$

where C_{fi} is the interfacial drag coefficient replacing the liquid drag coefficient C_D, and A_i is the interfacial area replacing the effective area A_{eff}. A_i can be expressed as

$$A_i = \pi d_N L_A \tag{77}$$

where L_A is the characteristic length of annular flow regime. Substituting equation (77) into equation (76) and rearranging, we have

$$L_A = \frac{1}{2}\,\frac{1}{C_{fi}}\,\frac{1}{\left[1 - \dfrac{Q_f}{Q_g}\,\dfrac{A_N}{A}\right]^2}\,d_N \tag{78}$$

For very high gas flow rate, i.e. for

$$\frac{Q_f}{Q_g}\,\frac{A_N}{A} \ll 1 \tag{79}$$

we have

$$L_A = \frac{1}{2}\,\frac{d_N}{C_{fi}} \tag{80}$$

For $L_A/D \gg 1$, that is, for

$$\frac{L_A}{D} = \frac{1}{2C_{fi}}\,\frac{d_N}{D} \gg 1 \tag{81}$$

the jet flow is expected to extend over a substantial length in a pipe until it disrupts. When the nozzle (or jet) diameter approaches the pipe diameter, the jet flow would continue as annular flow until it changes into annular/mist flow due to the growth of the most unstable disturbances, although the liquid film in this case is expected to be substantially thicker than that in the conventional annular two-phase flow under normal gravity. This can also be inferred from the results of Lee and Chan's linear stability analysis of cylindrical liquid sheets (ref. 19), where the cylindrical liquid jet structure is found to change from stable to wavy, wavy mist, and mist flow structure depending on the relative velocity of the gas and liquid phases. Since equation (81) is satisfied for low values of C_{fi} and larger values of d_N/D, the existence of annular flow structure is thus possible for very high relative velocities between the phases and for relatively larger nozzle diameter. In the T-shape two-phase mixer where the pipe diameter for gas phase is large, we can expect the appearance of annular flow. In some two-phase flow high gas flow experiments where gas is injected through multiple nozzles (or multiple holes) around the pipe periphery, the merger of jet flow from each hole would result in an annular flow structure. In any case, for high gas flow rates the annular flow is expected to change into wavy annular, annular mist, or mist flow far downstream due to the growth of the most unstable disturbances at the interfaces.

When $L_A/D \gtrsim 1$, i.e., when the jet length is not large, the jet would break down within a short distance from the nozzle exit and would appear as mist or fog, as is indicated from equation (75).

To determine the jet length L_A in equation (80), it is essential to first determine the interfacial friction coefficient C_{fi}. A number of relationships for the interfacial friction coefficient under normal gravity have been proposed (refs. 20 to 22). However, until the roles of such mechanisms as droplet entrainment flux, interfacial shear stress and turbulence in microgravity are better understood in two-phase flow, there will not be complete confidence in such correlations.

When the liquid flow rate is high enough such that equation (79) is not satisfied, i.e., for

$$\frac{Q_f}{Q_g}\frac{A_N}{A} \lesssim 1 \tag{82}$$

the jet length, L_A, calculated from equation (80) is expected to be very large. This can be explained physically. When the liquid phase velocity is comparable to the gas jet velocity, the disturbances move almost as fast as the liquid, and the jet structure can be sustained for a substantial distance downstream of the nozzle.

8.3 Breakup Due to Liquid Turbulence

Due to the very high level of turbulent fluctuations of liquid flow and the mutual influence of disturbances on each phase as mentioned earlier, a jet meeting the conditions of equation (82) may be disrupted or changed in some way. Let us look at the possible disruption of gas jet due to strong liquid turbulence. If the kinetic pressure of liquid turbulence is dominant over the capillary pressure of gas jet, i.e., when

$$\frac{f}{4}\rho_f U_f^2 > \frac{2\sigma}{d_N} \tag{83a}$$

or

$$We > 85.1\ Re^{1/5}\left(\frac{d_N}{D}\right)^{-1} \tag{83b}$$

the breakdown of gas jet structure is expected and the resulting flow would appear as dispersed or transitional bubbly-slug flow. When the turbulent fluctuation is not strong enough to disrupt the jet flow, i.e., when

$$We \leq 85.1\ Re^{1/5}\left(\frac{d_N}{D}\right)^{-1} \tag{84}$$

we expect strong waviness of jet flow or pinchoff of jet structure due both to strong turbulent fluctuations and to the growth of the most unstable disturbances. The resulting flow pattern may appear as wavy annular or more likely transitional annular-slug flow structure.

9. COMPARISONS AND DISCUSSION

A summary of the flow regime transition criteria for gas-liquid two-phase flows described is given in table I. (A more detailed summary, providing an outline of the reasoning, is given in tables II and III.) The flow regime transitions derived herein are based on the dominant physical mechanisms at given

conditions in a microgravity environment. Due to the assumptions and simplifications made in the derivations, a validation against experimental data is required.

Recently some experimental data for the gas-liquid two-phase flow in microgravity has been published. A direct comparison with this analysis is not possible because the inlet configurations (mixers) used in these experiments involve injecting the gas through multiple holes around the periphery of the pipe wall. However, a comparison can be made by adjusting the parameters of the analysis which are affected by the inlet geometry. The experimental data used in these comparisons are the air-water data of Lee (ref. 23), Dukler et al. (ref. 24), and Colin et al. (ref. 12).

Numerous two-dimensional flow regime maps for two-phase flow, both empirically and experimentally based, have been reported in the literature over the last several decades. Empirical maps prepared for one set of conditions are not necessarily valid for other geometries and properties. Theoretical flow regime maps have demonstrated some predictive success, but still remain to be proved. There thus are no generally accepted criteria for transition between the various flow regimes.

It is noted from table I that the physical conditions and transition criteria include geometric properties as well as physical properties. In addition, under the same physical condition, different transition criteria predict different flow regimes for the same dimensionless parametric values. This implies that the current flow regime maps based on two-dimensional coordinates may not be adequate to depict the whole physical flow regime and that some important parameters or physical mechanisms described by such parameters may be overlooked in such a map.

There has been a tendency to use the existing 1-g flow regime transition criteria to predict flow regimes in a microgravity environment. These criteria have yet to be demonstrated. Keeping these things in mind, comparisons are made with recently published experimental data in flow regime maps, prepared separately for each set of data. Superficial liquid and vapor velocities are chosen as coordinates to avoid tedious calculations to convert the original data. For comparison purposes only, the following adjustments are made to determine the values of some related parameters obtained from the analysis.

9.1 Determination of Drag Coefficient, C_D

The behavior of fluid spheres such as drops and bubbles differs from solid spheres primarily due to internal circulation and deformation. Internal circulation delays the onset of flow separation and wake formation in the external flow and decreases the drag exerted by the external flow. Internal circulation is negligible for high values of viscosity ratio, $\bar{\mu} = \mu_d/\mu_c$ where the subscripts d and c represent dispersed and continuous phase, respectively. Surface active contaminants can also eliminate the internal circulation, thereby significantly increasing the drag. Systems which exhibit high interfacial tension such as air/water and liquid metal/air are most subject to this effect. When a fluid sphere exhibits little internal circulation either because of high viscosity ratio or because of surface contamination, the external flow is indistinguishable from that around a solid sphere at the same Re_B.

Significant deformation from the spherical shape occurs in fluid spheres for large Re_B (e.g., for drops and bubbles rising or falling freely with $Re_B > 600$); this deformation tends to increase the drag. The presence of the walls also tends to cause deformation of a fluid sphere for values of $D_b/D \geq 0.3$ and as with solid spheres, the drag force tends to increase as D_b/D increases, though the effect is less than for a solid sphere under corresponding conditions.

Considering that the presence of surface-active contaminants is almost inevitable for every system, and that deformation from a spherical shape is expected for large Re_B, there is a significant difference in the value of C_D between the uncontaminated, spherical bubble and contaminated, deformed bubble. However, there appears to be insufficient data available regarding C_D of a bubble in a bounded regime as to allow a useful quantitative generalization to be drawn. Thus in the first category of physical condition where Re_B is expected large, the value of C_D is assumed to be that of a solid sphere at the same Re_B. One thing to be noted is that from equation (19), the value of C_D depends on the bubble diameter D_b which in turn depends on the value of C_D, thus some iterative calculations are needed to determine both values. In the second category of physical condition, as the size of bubble is determined by the growth mechanism where the bubble motion is supposed to be slow, C_D is assumed to be 18.3; this is the value given by Clift et al. (ref. 9) for $Re_B = 1.0$ and $\bar{\mu} = 0$.

9.2 Virtual Mass Coefficient, C_M

In the stationary system of bubble formation, some researchers have used the value of 11/16 for C_M (refs. 4, 27, and 28) while others have used 1/2 (refs. 29 and 30). Recently, Kim (ref. 3) analytically studied the added mass coefficient of a fluid sphere of diameter D_b moving with velocity U_f through a continuous liquid phase in square cross section channels for both coflowing and cross-flowing cases. He showed that C_M varies only with the diameter ratio D_b/D_p where D_p is the hydraulic diameter of the channel. According to his calculations, $0.5 \leq C_M \leq 1.0$ for $0 < D_b/D_p \leq 0.9$. Since from equation (59) D_b and C_M depend on each other, an iterative calculation would also be needed here. To avoid this iterative calculation, the value of 11/16 is adopted for C_M.

9.3 Interfacial Friction Coefficient, C_{fi}

As was mentioned earlier, there have been a number of reported relationships for C_{fi} under normal gravity. However, as it is not clear whether these formulations are valid in the present situation, and considering that the gas jet is highly turbulent, C_{fi} is taken to be 0.005, which is the value of friction factor for the turbulent flow in rough pipes.

9.4 Other Parameters

While a single nozzle configuration is considered in the present analysis, experiments conducted to date have used multiple nozzles. Thus the volumetric flow rate of gas for single nozzle, Q_g, is expressed as $Q_g = Q_g'/n$, where Q_g' is the total volumetric flow rate of gas for the system and n is the number of nozzles. In addition, the multiple nozzle systems are very close to cross-flowing systems, and as a result the coefficient for surface tension force $f(\varphi)$ in equation (1c) would differ from the value of 1, which is appropriate for a coflowing system. According to Kim (ref. 3), in a cross-flowing system the component of $f(\varphi)$ in the liquid flowing direction is given as $f(\varphi) = \sin\varphi/\varphi$. His calculation shows that the bubbles in a cross-flowing system detach at $\varphi = 45° \sim 50°$ giving $f(\varphi) \approx 0.9$. This value is used for multiple nozzle systems.

9.5 Comparison and Discussion

Since each physical condition represents a dominant physical mechanism, for demarcation purposes two vertical lines are drawn in figures 3 to 5, one at a value of U_g which satisfies the relation

$\rho_g\ (Q_g^2/A_N) = 0.1\ \sigma\pi d_N f(\varphi)$ (for the physical condition $\rho_g\ (Q_g^2/A_N) \ll \sigma\pi d_N f(\varphi)$), and the other at $\rho_g\ (Q_g^2/A_N) = 10\ \sigma\pi d_N f(\varphi)$ (for $\rho_g\ (Q_g^2/A_N) > \sigma\pi d_N f(\varphi)$). The appropriateness of these demarcations needs to be verified. The demarcation thus given divides the flow regime into three regions: the left-hand side region represents the region where first physical condition applies, an intermediate region for the second physical condition, and the right-hand side region for the third physical condition.

Figure 3 compares prediction from the present analysis with Dukler et al.'s drop tower data (ref. 24). (Comparisons with their learjet data was not considered because the mixer configuration used in those experiments differed significantly from the one used in this analysis. In the experiments liquid is injected through holes around the periphery of the pipe while gas is flowing through the pipe.)

In the region of first physical condition, the transition from dispersed to slug flow is obtained from equation (21), with C_D values based on the bubble Reynolds number Re_B. At the dispersed-slug flow transition, the bubble size is expected to be of the same order as the pipe diameter, $D_b \approx D$. Based on the pipe diameter, Re_B from experimental data lies in the range $100 \le Re_B \le 1000$ and values of C_D for these Reynolds numbers are $0.55 \le C_D \le 1.0$ (ref. 9). The transition lines are shown for low (0.55) and high (1.0) values of C_D. Comparison shows good agreement with the experimental data except for one slug flow point that is predicted to be dispersed flow.

In the region of second physical condition, the transition line $\sqrt{Q_f/Q_g} = 1.10$ is given empirically by Dukler et al. for the dispersed-slug flow transition; the transition line $\sqrt{Q_f/Q_g} = 2.0$ is from the present analysis. The transition line for the present analysis is derived as follows: Under the given experimental condition the bubble breakup condition equation (54) is not satisfied and the dispersed-slug transition criterion needs to be determined from the inequality condition. $\sqrt{Q_f/Q_g} \gg 0.4$ from equation (56). Representing equation (56) as $\sqrt{Q_f/Q_g} \ge 4.0$, and correcting the gas flow rate Q_g for the number of nozzles (four) yields the relation $\sqrt{Q_f/Q_g} \ge 2.0$, which is shown in the figure. This transition criterion occurs at somewhat higher value of $\sqrt{Q_f/Q_g}$ than the empirical value. This is probably due to a lack of proper accounting for the bubble formation and interaction phenomena of multiple nozzle system by the simple algebraic treatment of an inequality transition criterion. But, as will be mentioned later, the slug-dispersed flow transition in this region is still a big issue to be resolved.

The slug-annular flow transition is obtained from the condition of equation (52). In this case the gas flow rate is not modified by the number of nozzles. The reason for this is that in the dispersed-slug flow transition, the bubble size at detachment (which primarily depends on the gas flow rate at the nozzle) occurs as a result of the coalescence of big bubbles either in single nozzle or multiple nozzle systems. Thus it is the overall gas flow rate, rather than the gas flow rate at each nozzle, that determines the transition. If the number of nozzles is incorporated, the transition line for the slug-annular flow transition is somewhat lowered; this does not contradict the current comparison. However, no available data exists to clarify this point.

Figure 4 shows the comparison of the prediction with the KC-135 experiment data of Colin et al. (ref. 12). In their experiment, air is injected through eight holes of 1 mm diameter located uniformly around the periphery of a venturi-shaped section with a minimum diameter of 2 cm. The divergent

section length is 25 cm and the test section diameter is 4 cm. To study the inlet effect the minimum venturi-section diameter was used, because the liquid velocity there significantly differs from that in the test section. In the region of first physical condition, the transition for dispersed-slug flow is obtained using the representative value of $C_D = 0.5$ for a value of Re_B on the order of 10^4. As can be seen the comparison shows very good agreement. In the region of second physical condition, the transition for dispersed-slug flow is given empirically by the authors as $\sqrt{Q_f/Q_g} = 1.79$. For comparison, Dukler et al.'s transition criterion and that from the present analysis are also shown. (The criterion from the present analysis is obtained similarly to the one in fig. 3 except that the number of nozzles is 8 instead of 4.) Also shown is the slug-annular transition from the present analysis. Colin et al.'s transition criterion lies at a somewhat higher value of $\sqrt{Q_f/Q_g}$ than that of Dukler et al. and the present criterion lies in between them. Colin et al. explained Dukler et al.'s lower value as arising from suppressed bubble coalescence due to the reduced turbulence level in the smaller tube Dukler et al. used. Considering that the data of both experiments in the second category of physical condition are subject to bubble coalescence (under the criterion of eq. (55)), two more reasons seem to be plausible for this difference; first, in the Colin et al.'s experiment, the retardation of liquid velocity from the venturi section to the test section may jam together bubbles near the entrance region of the test section and thereby enhance bubble coalescence. Second, due to the relatively short length-to-diameter ratio in Dukler et al.'s experiment, the coalescence of bubbles may not be complete and more coalescence might be expected if the tube were longer. This means that the flow regime may not be fully established at the test section exit. More detailed study of these issues is needed in the future.

Figure 5 shows comparison of the present prediction with Lee's adiabatic air-water data from KC-135 experiments. Since details are not given regarding the configuration of the inlet geometry, a direct comparison is not possible. But for comparison purposes, the nozzle diameter is arbitrarily assumed to be 1 mm. This arbitrariness of choosing nozzle diameter surely influences the demarcation of physical conditions and the relevant transition criteria under the given physical condition. The primary reason for making this comparison is because his experiment is the only one that contains annular flow regime data against which the comparison of the present prediction for the annular flow regime is possible. The demarcation of the physical condition in the figure is shown for $d_N = 1$ mm and $f(\varphi) = 0.9$. In the region of first physical condition, the value of C_D is taken to be 0.55; this value is basically a constant for solid spheres with Reynolds number on the order of 10^3. Two data points available in this region show good agreement. But it is suspicious because their locations are subject to nozzle diameter. In the region of third physical condition, annular flow regime data agrees well with the prediction. The arbitrarily chosen nozzle diameter for this data affects only the value of physical condition and not the liquid superficial velocity (or the ratio of the flow rate); the annular data points nearest the demarcation line would still be predicted to be annular even if they fell in the intermediate range of physical condition. Some wavy annular flow pattern was reported. This was predicted as a possibility in sufficiently long pipes under the third physical condition in the analysis.

In figure 6 are all the above experimental data plotted in a $\sqrt{Q_f/Q_g}$ versus $[\rho_g(Q_g^2/A_N)]/\sigma\pi d_N f(\varphi)$ map. The abscissa, which is a dimensionless physical condition, is analogous to the Weber number in terms of average gas nozzle velocity and nozzle diameter. The main purpose for this is to see if any definite trend among data exist in terms of the two most important dimensionless parameters adopted herein. First of all, it is seen from the figure that the data are grouped into three distinctive regions which are defined by the two demarcation lines. All the data (except one slug flow data from Colin et al.) on the left-hand side of demarcation, $[\rho_g(Q_g^2/A_N)]/\sigma\pi d_N f(\varphi) = 0.1$, represent dispersed flow. It is interesting to note at this point that according to equation (26), slug flow is not possible

unless the liquid flow rate is significantly small; that condition may imply an unrealistically small flow rate in an actual experiment. All of Lee's data which falls on the right-hand side of the demarcation, $[\rho_g(Q_g^2/A_N)]/\ \sigma\pi d_N f(\varphi) = 10$, represents annular flow. Colin et al's two slug flow data in this region may be suspect because the gas flow rates for these points are unusually high, more than twice as large as the rates for the largest value of their other slug flow data. In the intermediate region between the demarcations, dispersed and slug flow data exist together and the transitions for dispersed to slug flow are given from Colin et al., Dukler et al., and the present prediction (nozzle number, $n = 8$). Also shown is the slug-annular flow transition criterion from the present analysis. It seems that the demarcation by physical condition could be used to establish the sole existence of dispersed or annular flow structure. In the intermediate region, the transition criterion for dispersed to slug flow could be used to predict critical void fraction. Since the data are not extensive and some may doubt the quality of data, it is dangerous to draw any conclusion. However, the above flow regime map based on the volumetric flow ratio and dimensionless physical condition appears to be instructive and could be used to better predict the two-phase flow regime in microgravity, including the effect of inlet geometry.

The comparisons made above are generally satisfactory even though rough estimations are made for some physical parameters. More extensive data are required to properly define the demarcations for each physical condition and transition criteria in each category of physical condition.

CONCLUSIONS

An attempt has been made to predict the gas-liquid two-phase flow regime in a pipe with simple inlet geometry in microgravity through a scaling analysis based on the dominant physical mechanisms.

The present analysis has clarified much of the physics involved in such problems, especially the effect of inlet geometry on the flow regime transition.

Comparisons of the predictions with the existing experimental data show good agreement. However, further work is required to better define some physical parameters.

The present analysis is capable of being applied to other configurations and seems to be a good first step in resolving the unknowns that have confronted researchers on this subject since its inception: How are phases distributed spatially in microgravity and what is the effect of inlet geometry on this process?

APPENDIX

Kolmogrov (ref. 29) and Hinze (ref. 10) showed that the splitting of a drop or bubble in turbulent flow will depend upon a critical Weber number of liquid flow. Hinze correlated the maximum or critical bubble or drop diameter which is stable under turbulent fluctuations as

$$D_{bc} = K\left(\frac{\sigma}{\rho_c}\right)^{3/5} \varepsilon^{-2/5} \tag{A-1}$$

where ε is the rate of energy dissipation per unit mass and K is a constant related to the critical Weber number. Hinze determined $K = 0.725$ based on the experimental data of Clay (ref. 30) for droplet breakup in a turbulent flow between coaxially rotating cylinders. Later Sevik and Park (ref. 11) theoretically predicted $K = 1.14$ by considering the resonance of the liquid drops and gas bubbles. Their prediction shows remarkable agreement with their experimental value of $K = 1.15$, which was obtained from the breakup of air bubbles in a turbulent water jet, by setting a characteristic frequency of the turbulence equal to bubble's resonant frequency. One thing that should be noted is that the relationship, equation (A-1), is based on the condition of noncoalescence of bubbles which is possible only at very low concentration of air bubbles. Adopting the value for $K = 1.14$ and following Levich (ref. 8), the rate of energy dissipation per unit mass can be expressed

$$\varepsilon = \frac{2f}{D} U_f^3 \tag{A-2}$$

Substituting equation (A-2) into equation (A-1) and predicting the friction coefficient f from the Blasius equation, we obtain

$$\frac{D_{bc}}{D} = 2.96\ We^{-3/5} Re^{2/25} \tag{A-3}$$

Under the bubble breakup conditions, equations (54) and (64), which are possible for very high value of Q_f or Re, it can be shown that $D_{bc}/D < 1$ in equation (A-3) through comparison of equation (A-3) with equations (54) and (64). This indicates that whenever bubble breakup occurs, the critical bubble is a small, dispersed bubble and, without coalescence, the flow regime would be dispersed flow.

Taitel et al. (ref. 31) expressed the energy dissipation rate per unit mass ε and the friction factor f in terms of the mixture velocity and liquid kinematic viscosity for the transition criterion between bubble and slug flow regime. However, no physical explanation was given to support this formulation.

REFERENCES

1. Mahefkey, E.T., "Thermal Management Issues and Technology Needs for SDI," AIAA 22nd Thermophysics Conference, Honolulu, Hawaii, AIAA-87-1478, June 1987.

2. Taitel, Y.G and Dukler, A.E., "A Model for Predicting Flow Regime Transitions in Horizontal and Near Horizontal Gas-Liquid Flow," AIChE J, Vol. 22, pp. 47-55, 1976.

3. Kim, I.W., "Modelling of Bubble and Drop Formation in Flowing Liquids in Microgravity," Ph.D Thesis, May 1992, Case Western Reserve University.

4. Kumar, R. and Kuloor, N.R., "The Formation of Bubbles and Drops," Advances in Chemical Engineering, Vol. 8, 1970, Academic Press.

5. Kupferberg, A. and Jameson, G.J., "Bubble Formation at a Submerged Orifice Above a Gas Chamber of Finite Volume," Trans. Instn. Chem. Engrs., Vol. 47, pp. T241-T250, 1969.

6. Walters, J.K. and Davidson, J.F., "The Initial Motion of a Gas Bubble Formed in an Inviscid Liquid, Part 2. The Three-Dimensional Bubble and the Toroidal Bubble," JFM Vol. 17, Pt 3, pp. 321-336, 1964.

7. McCann, D.J. and Prince, R.G.M., "Regimes of Bubbling at a Submerged Orifice," Chem. Engr. Sci., Vol. 26, pp. 1505-1512, 1971.

8. Levich, V.G., "Physicochemical Hydrodynamics," 1962, Prentice-Hall.

9. Clift, R., Grace, J.R., and Weber, M.E., "Bubbles, Drops, and Particles," 1978, Academic Press.

10. Hinze, J.O., "Fundamentals of the Hydrodynamic Mechanism of Splitting in Dispersion Processes," AIChE J, Vol. 1, No. 3, pp. 289-295, 1955.

11. Sevik, M. and Park, S.H., "The Splitting of Drops and Bubbles by Turbulent Fluid Flow," J. Fluids Engr., pp. 53-60, Mar. 1973.

12. Colin, C., Fabre, J., and Dukler, A.E., "Gas-Liquid Flow at Microgravity Conditions - I," Int. J. Multiphase Flow, Vol. 17, No. 4, pp. 534-544, 1991.

13. Smith, S.W.J. and Moss, H., "Experiments With Mercury Jets," Proc. Roy. Soc. A93, pp. 373-393, 1917.

14. Scheele, G.F. and Meister, B.J., "Drop Formation at Low Velocities in Liquid-Liquid Systems: Part II. Prediction of Jetting Velocity," AIChE J, Vol. 14, No. 1, pp. 15-19, 1968.

15. Ostrach, S. and Koestel, A., "Film Instabilities in Two-Phase Flows," AIChE J, Vol. 11, No. 2, pp. 294-303, 1965.

16. Meister, B.J. and Scheele, G.F., "Prediction of Jet Length in Immiscible Liquid System," AIChE J, Vol. 15, No. 5, pp. 689-699, 1969.

17. Leibson, I., Holocomb, E.G., Cacoso, A.G., and Jacmic, J.J., "Rate of Flow and Mechanics of Bubble Formation from Single Submerged Orifices," AIChE J, Vol. 2, No. 3, pp. 296-306, 1956.

18. Hayworth, C.B. and Treybal, R.E., "Drop Formation in Two-Liquid-Phase Systems," Ind. Eng. Chem., Vol. 42, No. 6, pp. 1174-1181, 1950.

19. Lee, J.G. and Chen, L.D., "Linear Stability Analysis of Gas-Liquid Interface." AIAA J. Vol. 29, No. 10, pp. 1589-1595, 1991.

20. Wallis, G.B., "One-Dimensional Two-Phase Flow," 1969, McGraw-Hill Book Co.

21. Asali, J.C., Hanratty, T.J. and Andreussi, P., "Interfacial Drag and Film Height for Vertical Annular Flow," AIChE J, Vol. 31, pp. 895-902, 1985.

22. Ambrosini, W., Andreussi, P., and Azzopardi, B.J., "A Physically Based Correlation for Drop Size in Annular Flow," Int. J. Multiphase Flow, Vol. 17, No. 4, pp. 497-507, 1991.

23. Lee, D., "Thermohydraulic and Flow Regime Analysis for Condensing Two-Phase Flow in a Microgravity Environment," Ph.D. Thesis, Dec. 1987, Texas A & M University.

24. Dukler, A.E., Fabre, J.A., McQuillen, J.B., and Vernon, R., "Gas-Liquid Flow at Microgravity Conditions: Flow Patterns and Their Transitions," Int. J. Multiphase Flow, Vol. 14, No. 4, pp. 389-400, 1988.

25. Davidson, J.F. and Schüler, B.O.G., "Bubble Formation at an Orifice in an Inviscid Liquid," Trans. Instn. Chem. Engrs., Vol. 38, pp. 335-342, 1960.

26. Geary, N.W. and Rice, R.G., "Bubble Size Prediction for Rigid and Flexible Spargers," AIChE J, Vol. 37, No. 2, pp. 161-168, 1991.

27. Davidson, J.F. and Harrison, D., "Fluidised Particles," 1963, Cambridge University Press.

28. Rice, R.G. and Howell, S.W., "Bubble Formation from Elastic Holes," Chem. Eng. Commun., Vol. 59, p. 229, 1987.

29. Kolmogorov, A.N., "On the Disintegration of Drops in a Turbulent Flow," Doklady Akad. Nauk., SSSR, Vol. 66, p. 825, 1949.

30. Clay, P.H., "Proceedings of the Royal Academy of Science (Amsterdam)," Vol. 43, p. 852, 1940.

31. Taitel, Yl, Bornea, D., and Dukler, A.E., "Modelling Flow Pattern Transitions for Steady Upward Gas-Liquid Flow in Vertical Tubes," AIChE J, Vol. 26, No. 3, pp. 345-354, 1980.

TABLE I.—SUMMARY OF THE ANALYSIS

Physical condition		Transition criterion		Flow regime
$\rho_g \frac{Q_g^2}{A_N} \ll \sigma\pi d_N$		$We^{1/2} > \left(\frac{8}{C_D}\right)^{1/2}\left(\frac{d_N}{D}\right)^{1/2}$		Dispersed
		$We^{1/2} \leq \left(\frac{8}{C_D}\right)^{1/2}\left(\frac{d_N}{D}\right)^{1/2}$		Slug
$\rho_g \frac{Q_g^2}{A_N} \lesssim \sigma\pi d_N$	$\frac{Q_g}{Q_f}\frac{A}{A_N} \leq 0.025\ C_D \frac{\rho_f}{\rho_g}$	$\sqrt{\frac{Q_f}{Q_g}} \gg 0.4$		Dispersed
		$\sqrt{\frac{Q_f}{Q_g}} > 0.4$	$We > 870\sqrt{\frac{Q_f}{Q_g}}\ Re^{1/5}$	Dispersed
			$We < 870\sqrt{\frac{Q_f}{Q_g}}\ Re^{1/5}$	Slug
		$\sqrt{\frac{Q_f}{Q_g}} \leq 0.4$	$We > 870\sqrt{\frac{Q_f}{Q_g}}\ Re^{1/5}$	Slug or churn
			$We < 870\sqrt{\frac{Q_f}{Q_g}}\ Re^{1/5}$	Annular

TABLE I.—Concluded.

Physical Condition		Transition criterion			Flow regime
$\rho_g \frac{Q_g^2}{A_N} \lesssim \sigma\pi d_N$	$\frac{Q_g}{Q_f}\frac{A}{A_N} > 0.025\ C_D \frac{\rho_f}{\rho_g}$	$\left(1 + C_M \frac{\rho_f}{\rho_g}\right)^{1/2} \frac{d_N}{D} \ll 2\sqrt{3}$			Dispersed
		$\left(1 + C_M \frac{\rho_f}{\rho_g}\right)^{1/2} \frac{d_N}{D} < 2\sqrt{3}$	$We > \frac{1205}{\left(1 + C_M \frac{\rho_f}{\rho_g}\right)^{1/2}} \frac{d_N}{D} Re^{1/2}$		Dispersed
			$We < \frac{1205}{\left(1 + C_M \frac{\rho_f}{\rho_g}\right)^{1/2}} \frac{d_N}{D} Re^{1/2}$		Slug
		$\left(1 + C_M \frac{\rho_f}{\rho_g}\right)^{1/2} \frac{d_N}{D} \geq 2\sqrt{3}$	$We > \frac{1205}{\left(1 + C_M \frac{\rho_f}{\rho_g}\right)^{1/2}} \frac{d_N}{D} Re^{1/2}$		Slug or churn
			$We < \frac{1205}{\left(1 + C_M \frac{\rho_f}{\rho_g}\right)^{1/2}} \frac{d_N}{D} Re^{1/2}$		Annular
$\rho_g \frac{Q_g^2}{A_N} > \sigma\pi d_N$		$\frac{Q_f}{Q_g}\frac{A_N}{A} \ll 1$ (jet)	$\frac{1}{2C_{fi}} \frac{d_N}{D} \gg 1$	Yes	Annular/ mist flow
				No	Mist flow
		$\frac{Q_f}{Q_g}\frac{A_N}{A} \lesssim 1$	$We > 85.1\ Re^{1/8}\left(\frac{d_N}{D}\right)^{-1}$		Dispersed or dispersed - slug flow
			$We \leq 85.1\ Re^{1/8}\left(\frac{d_N}{D}\right)^{-1}$		Wavy annular or annular - slug flow

TABLE II.—SUMMARY OF THE ANALYSIS FOR LOW AND INTERMEDIATE GAS FLOW RATES. (NUMBERS AT LEFT REFER TO APPLICABLE SECTIONS OF THE TEXT.)

Physical condition		Force balance used to determine departure size	Departure size $\frac{D_b}{D}$ and initial flow regime	Bubble coalescence in nozzle region?	Breakup due to liquid turbulence?	Downstream flow regime
4.1 $\rho_g \frac{Q_g^2}{A_N} \ll \sigma \pi d_N$ Gas inertia ≪ Surface tension		5.1 Viscous drag ~ Surface tension	5.1 $\left(\frac{8}{C_D}\right)^{1/2} We^{-1/2} \left(\frac{d_N}{D}\right)^{1/2} < 1 \rightarrow$ Dispersed	5.2 No	5.3 No	Dispersed
			5.1 $\left(\frac{8}{C_D}\right)^{1/2} We^{-1/2} \left(\frac{d_N}{D}\right)^{1/2} \geq 1 \rightarrow$ Slug	5.2 No	5.3 No	Slug
4.2 $\rho_g \frac{Q_g^2}{A_N} \lesssim \sigma \pi d_N$ Gas inertia ≲ Surface tension	7.4 $\frac{Q_g A}{Q_f A_N} \leq \frac{C_D}{40} \frac{\rho_f}{\rho_g}$ Inertial ≤ Viscous drag	6.1 Viscous ~ Momentum drag flux	6.1 $0.4 \left(\frac{Q_g}{Q_f}\right)^{1/2} \ll 1 \rightarrow$ Dispersed[a]	No effect on flow regime		Dispersed
			6.1 $0.4 \left(\frac{Q_g}{Q_f}\right)^{1/2} < 1 \rightarrow$ Dispersed	6.2 Yes	6.3 $\frac{We}{870} \left(\frac{Q_g}{Q_f}\right)^{1/2} Re^{-1/8} < 1 \rightarrow$ Yes	Dispersed
					6.3 $\frac{We}{870} \left(\frac{Q_g}{Q_f}\right)^{1/2} Re^{-1/8} > 1 \rightarrow$ No	Slug
			6.1 $0.4 \left(\frac{Q_g}{Q_f}\right)^{1/2} \geq 1 \rightarrow$ Slug	6.2 Yes	6.3 $\frac{We}{870} \left(\frac{Q_g}{Q_f}\right)^{1/2} Re^{-1/8} < 1 \rightarrow$ Yes	Slug or churn
					6.3 $\frac{We}{870} \left(\frac{Q_g}{Q_f}\right)^{1/2} Re^{-1/8} > 1 \rightarrow$ No	Annular
	7.4 $\frac{Q_g A}{Q_f A_N} > \frac{C_D}{40} \frac{\rho_f}{\rho_g}$ Inertial > Viscous drag	7.1 Inertial ~ Momentum drag flux	7.1 $\frac{1}{2\sqrt{3}} \left(1 + C_M \frac{\rho_f}{\rho_g}\right)^{1/2} \frac{d_N}{D} \ll 1 \rightarrow$ Dispersed[a]	No effect on flow regime		Dispersed
			7.1 $\frac{1}{2\sqrt{3}} \left(1 + C_M \frac{\rho_f}{\rho_g}\right)^{1/2} \frac{d_N}{D} < 1 \rightarrow$ Dispersed	7.2 Yes	7.3 $\frac{We}{1205} \left(1 + C_M \frac{\rho_f}{\rho_g}\right)^{1/2} \left(\frac{D}{d_N}\right) Re^{-1/2} > 1 \rightarrow$ Yes	Dispersed
					7.3 $\frac{We}{1205} \left(1 + C_M \frac{\rho_f}{\rho_g}\right)^{1/2} \left(\frac{D}{d_N}\right) Re^{-1/2} < 1 \rightarrow$ No	Slug
			7.1 $\frac{1}{2\sqrt{3}} \left(1 + C_M \frac{\rho_f}{\rho_g}\right)^{1/2} \frac{d_N}{D} \geq 1 \rightarrow$ Slug	7.2 Yes	7.3 $\frac{We}{1205} \left(1 + C_M \frac{\rho_f}{\rho_g}\right)^{1/2} \left(\frac{D}{d_N}\right) Re^{-1/2} > 1 \rightarrow$ Yes	Slug or churn
					7.3 $\frac{We}{1205} \left(1 + C_M \frac{\rho_f}{\rho_g}\right)^{1/2} \left(\frac{D}{d_N}\right) Re^{-1/2} < 1 \rightarrow$ No	Annular

[a]Very small bubbles.

TABLE III.—SUMMARY OF THE ANALYSIS FOR HIGH GAS FLOW RATES. (NUMBERS AT LEFT REFER TO APPLICABLE SECTIONS OF THE TEXT.)

Physical condition	Gas/liquid flow ratio; mechanism of possible jet instability	Jet breakup?	Flow regime
4.3 $\rho_g \frac{Q_g^2}{A_N} > \sigma\pi d_N$ Gas inertia > Surface tension	8.1, 8.2 $\frac{Q_f}{Q_g}\frac{A_N}{A} \gg 1$; Kelvin-Helmholtz instability	8.2 $\frac{1}{2C_{fi}}\frac{d_N}{D} \lesssim 1 \rightarrow$ Yes	8.2 Mist
		8.2 $\frac{1}{2C_{fi}}\frac{d_N}{D} \gg 1 \rightarrow$ No	8.2 Annular/mist
	8.1, 8.2, 8.3 $\frac{Q_f}{Q_g}\frac{A_N}{A} \lesssim 1$; Liquid turbulence	8.3 $\frac{We}{85.1} Re^{-1/5} \frac{d_N}{D} > 1 \rightarrow$ Yes	8.3 Dispersed or dispersed/slug
		8.3 $\frac{We}{85.1} Re^{-1/5} \frac{d_N}{D} < 1 \rightarrow$ No	8.3 Wavy annular or annular/slug

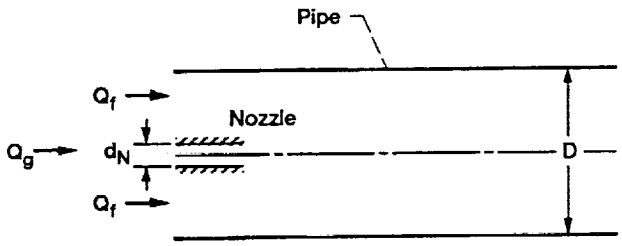

Figure 1.—Schematic of the system.

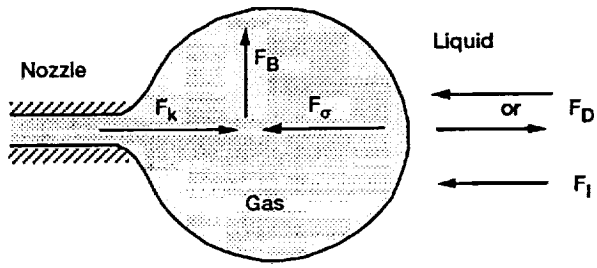

Figure 2.—Forces acting on a bubble.

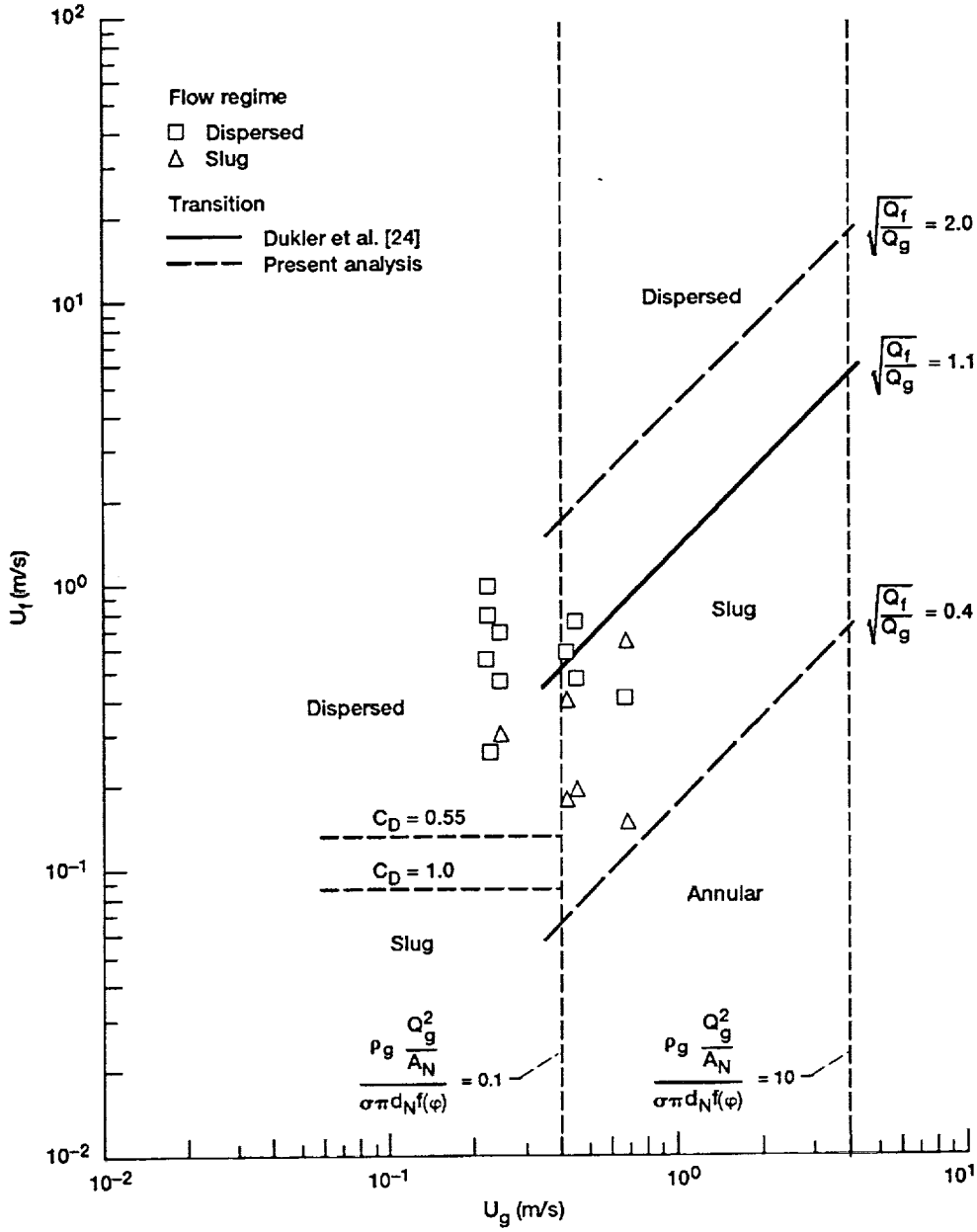

Figure 3.—Comparison of Dukler et al.'s data with the present transition criteria.

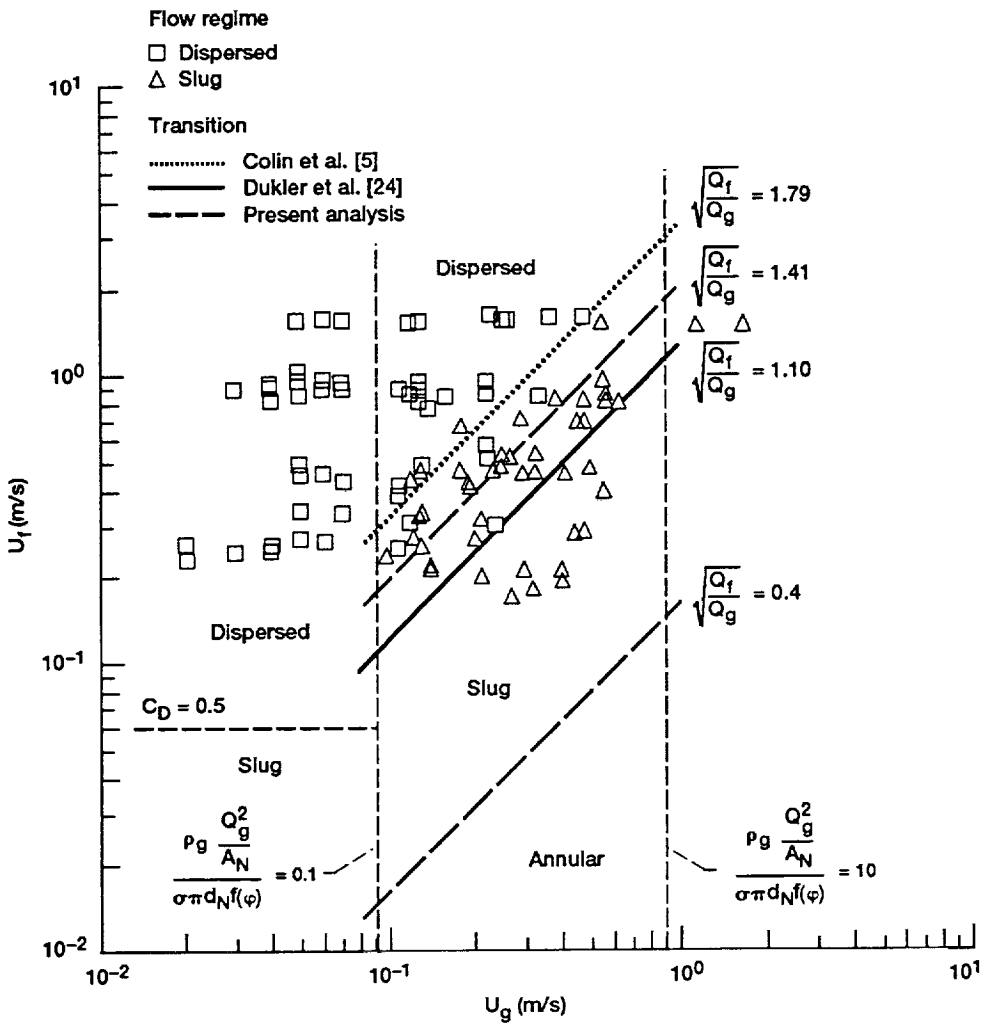

Figure 4.—Comparison of Colin et al.'s data with the present transition criteria.

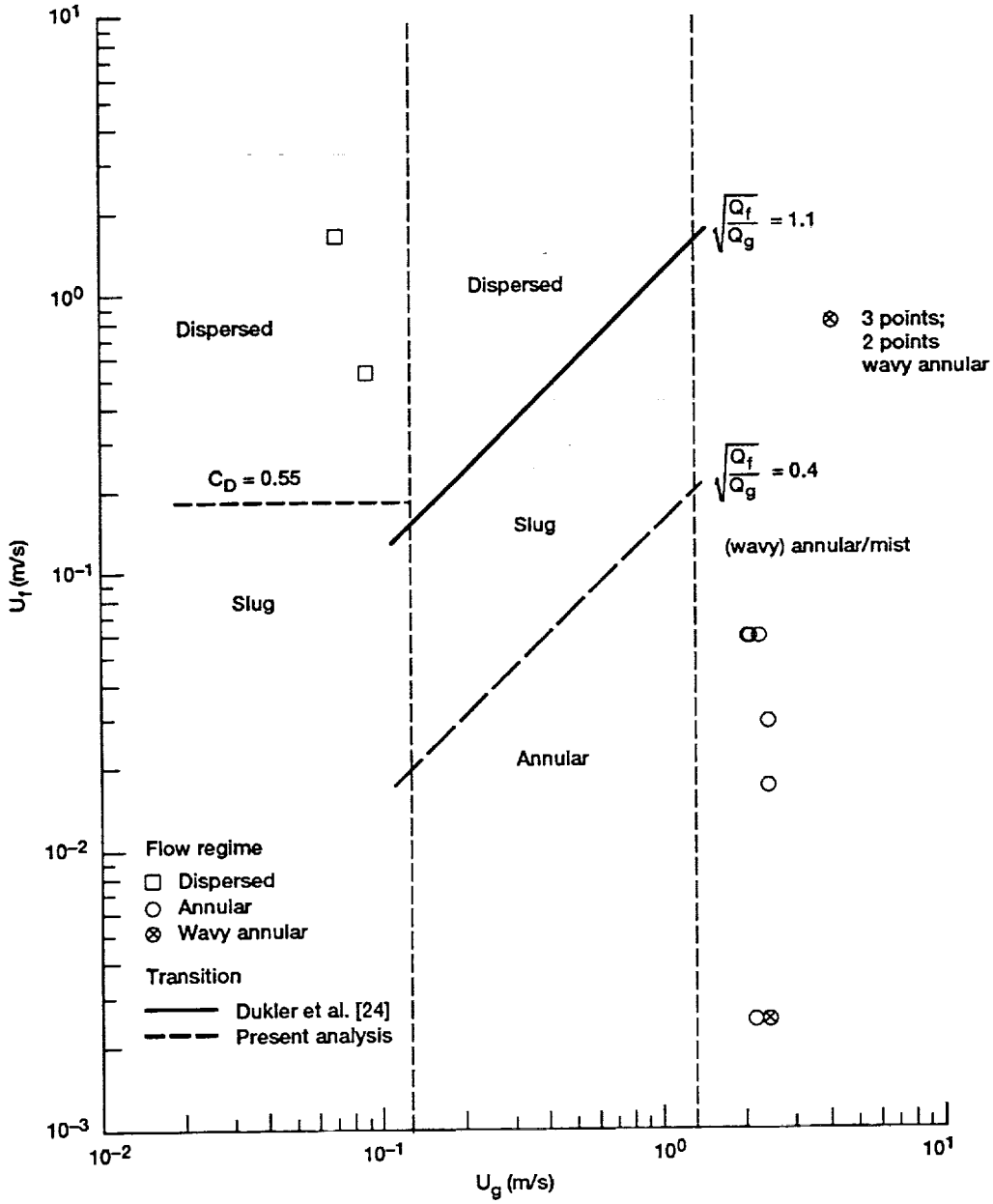

Figure 5.—Comparison of Lee's data with the present transition criteria.

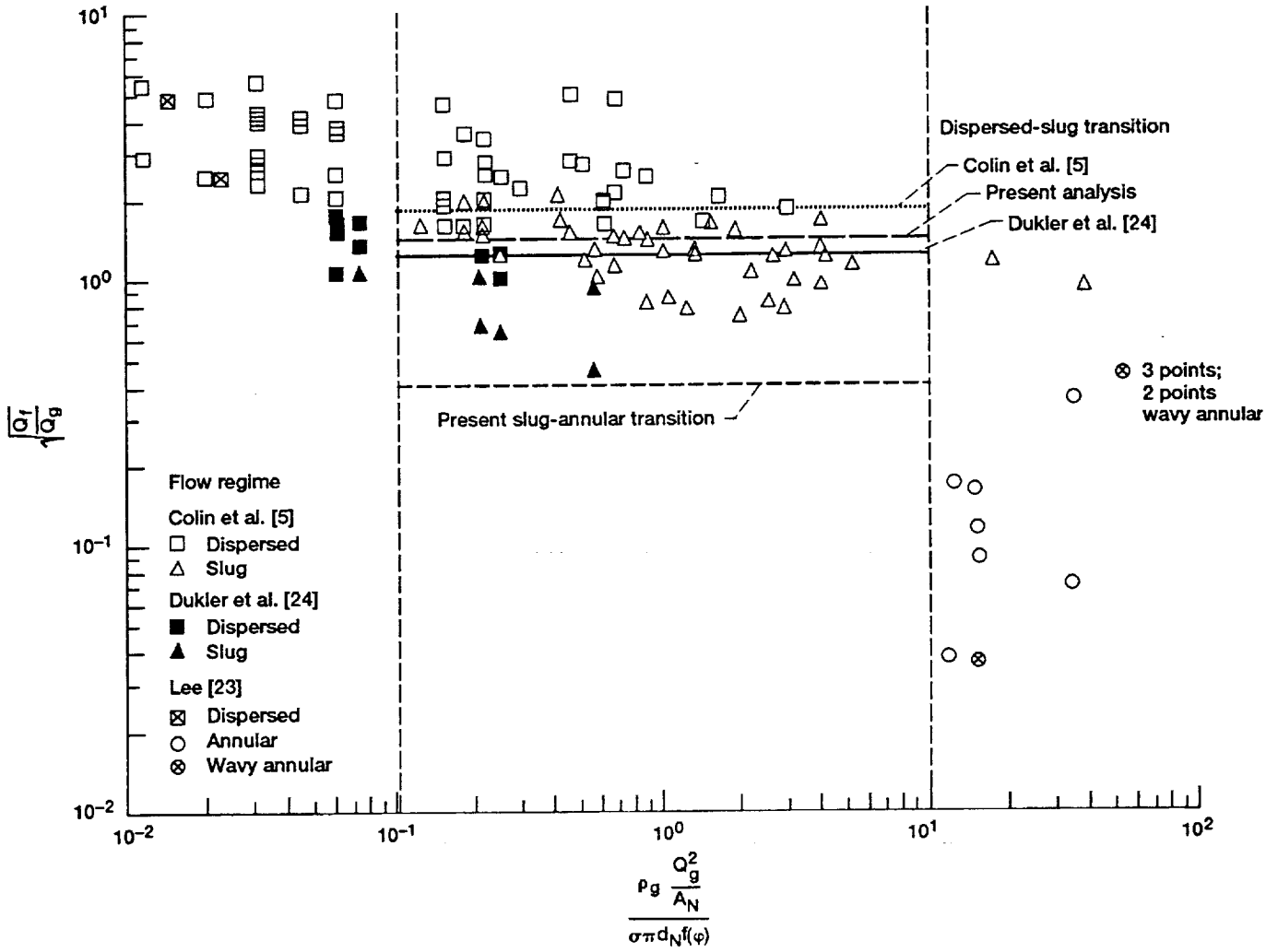

Figure 6.—Comparison of data under flow-regime map developed from the present analysis.

REPORT DOCUMENTATION PAGE

Form Approved
OMB No. 0704-0188

1. AGENCY USE ONLY (*Leave blank*)	2. REPORT DATE	3. REPORT TYPE AND DATES COVERED
	July 1993	Technical Memorandum

4. TITLE AND SUBTITLE

Prediction of Gas-Liquid Two-Phase Flow Regime in Microgravity

5. FUNDING NUMBERS

WU-694-03-0A

6. AUTHOR(S)

Jinho Lee and Jonathan A. Platt

7. PERFORMING ORGANIZATION NAME(S) AND ADDRESS(ES)

National Aeronautics and Space Administration
Lewis Research Center
Cleveland, Ohio 44135-3191

8. PERFORMING ORGANIZATION REPORT NUMBER

E-7079

9. SPONSORING/MONITORING AGENCY NAME(S) AND ADDRESS(ES)

National Aeronautics and Space Administration
Washington, D.C. 20546-0001

10. SPONSORING/MONITORING AGENCY REPORT NUMBER

NASA TM-106274

11. SUPPLEMENTARY NOTES

Jinho Lee, National Research Council and NASA Research Associate at Lewis Research Center; and Jonathan A. Platt, Lewis Research Center. Responsible person, Jonathan A. Platt, (216) 433-2862.

12a. DISTRIBUTION/AVAILABILITY STATEMENT

Unclassified - Unlimited
Subject Category ~~39~~ 29

12b. DISTRIBUTION CODE

13. ABSTRACT (*Maximum 200 words*)

An attempt is made to predict gas-liquid two-phase flow regime in a pipe in a microgravity environment through scaling analysis based on dominant physical mechanisms. Simple inlet geometry is adopted in the analysis to see the effect of inlet configuration on flow regime transitions. Comparison of the prediction with the existing experimental data shows good agreement, though more work is required to better define some physical parameters. The present analysis clarifies much of the physics involved in this problem and can be applied to other configurations.

14. SUBJECT TERMS

Two-phase flow; Microgravity; Scaling analysis

15. NUMBER OF PAGES
37

16. PRICE CODE
A03

17. SECURITY CLASSIFICATION OF REPORT	18. SECURITY CLASSIFICATION OF THIS PAGE	19. SECURITY CLASSIFICATION OF ABSTRACT	20. LIMITATION OF ABSTRACT
Unclassified	Unclassified	Unclassified	